06

Scanning nanoindentation as an instrument of studying local mechanical properties distribution in wood and a new technique for dendrochronology

© Yu.I. Golovin,[1,2] A.I. Tyurin,[1] A.A. Gusev,[1,3,4] S.M. Matveev,[1,3] D.Yu. Golovin,[1] A.A. Samodurov,[1] I.A. Vasyukova,[1] M.A. Yunak,[1] E.A. Kolesnikov,[4] O.V. Zakharova[1,4]

[1] Institute for Nanotechnology and Nanomaterials, G.R. Derzhavin Tambov State University, Tambov, Russia
[2] Moscow State University, Moscow, Russia
[3] Voronezh State University of Forestry and Technologies named after G.F. Morozov, Voronezh, Russia
[4] National University of Science and Technology MISiS, Moscow, Russia
e-mail: yugolovin@yandex.ru

Received November 23, 2021
Revised December 27, 2021
Accepted January 8, 2022

The paper presents the results of scanning of mechanical properties of coniferous (common pine *Pinus sylvestris*) and deciduous (small-leaved lime *Tilia cordata* and common oak *Quercus robur*) trees wood using nanoindentation on crosscut face. Manifold increase in microhardness H and Young's modulus E has been observed between early and late wood in every annual growth ring. Significant differences in intraring radial dependencies of H and E have been found among studied species. For all studied species the average values of E and H of early wood in each annual ring are found to be independent from ring width, while such dependence for late wood is weak at most. The ring widths measured by nanoindentation coincide with the ones measured by standard optical method within 2−3%. The developed technique and obtained results can be useful 1) to amend the understanding the origins of macromechanical properties of various wood species and their dependence upon microstructural characteristics and growth conditions, 2) to optimize the technologies of growing, reinforcement and subsequent usage of the wood, 3) to develop new independent high resolution methods in dendrochronology.

Keywords: nanoindentation, nano-/microhardness and Young's modulus scanning, tree annual growth rings, dendrochronology.

DOI: 10.21883/TP.2022.04.53605.297-21

Introduction

In the context of material physics, wood is a natural hierarchically-structured composite material with well-marked heterogeneity, anisotropy of all properties, and capacity for regeneration (curing of defects). Several scale-hierarchical levels may be distinguished (rather tentatively) in the structure of wood (Fig. 1): atomic-molecular level, nano- (nanocrystals and nanofibrils), micro- (microfibers, cell walls), meso- (cells, large vessels), and macrolevels (annual growth rings, structural macrodefects, cracks, etc.). Each of them produces its own contribution to the entire complex of physical and chemical properties.

Modern means and methods, which are traditionally used in physics of the solid state and material physics, have been applied in the studies of microstructure and properties of wood in the last 15 to 20 years [1]. The microstructure is examined with transmission and scanning electron microscopes, scanning probe microscopes (primarily atomic force ones), confocal laser microscopes, and optical microscopes in various modes [2–4]. The nature and degree of ordering of cellulose molecules in nanofibers is determined by X-ray diffractometry [5,6], synchrotron-based X-ray microscopy [7], and small-angle X-ray scattering. The elemental and phase compositions are identified by various spectroscopic techniques. Infrared (IR) and Fourier transform IR (FTIR) [8–10], Raman [10–12], Brillouin [13], and nuclear magnetic resonance [14] spectroscopy, X-ray fluorescence analysis [15], and other analytical methods are used. Comparative reviews of the capabilities of the most widely used physical methods for examining the molecular, subcellular, and cellular structure of wood have been published recently [16,17].

The mechanical properties of wood at nano- and microlevels are studied, just as in other materials, via nano- and micromechanical testing [18–21], typically with the use of atomic force microscopes [22–25] and nanoindentometers [26–34]. Specifically, the mechanical properties of individual nanofibrils and microfibers of cellulose [2,35–37] and cell walls [16,38–41] of various types of wood were examined with the use of nano- and micromechanical methods; a large set of intriguing data was obtained as

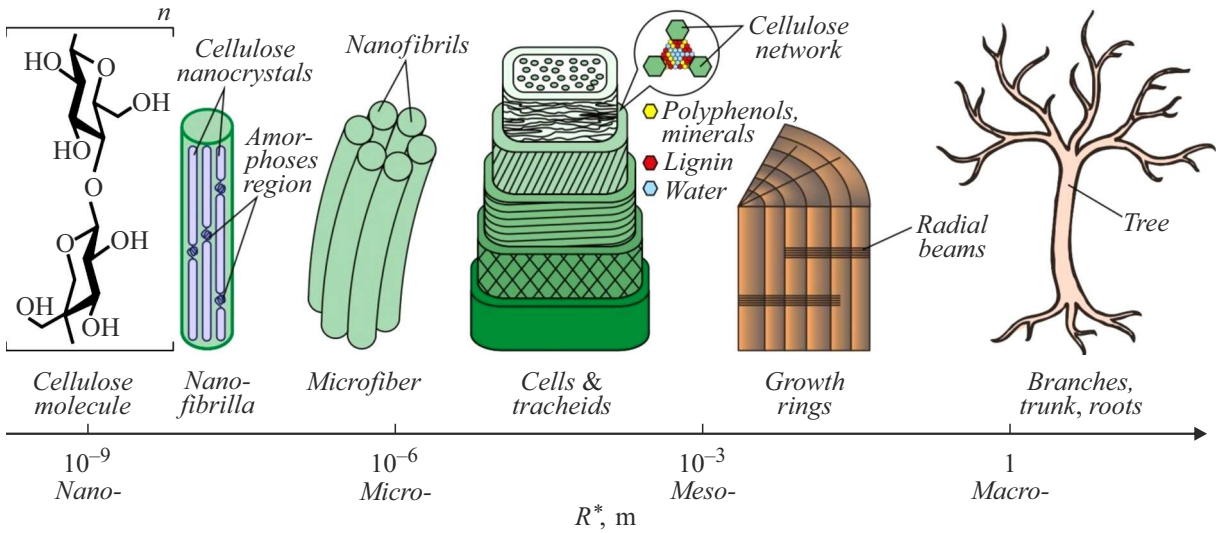

Figure 1. Scale-hierarchical levels of the structure of wood.

a result, but it corresponded to specific locations and elements of the nano- and microstructure and did not envision mapping of the mechanical properties of regions extending over several annual growth rings. Therefore, the relation between the properties of individual nano- and microstructural elements of wood and its macromechanical properties, the width of annual growth rings, the fraction of late wood in them, etc., remained unexamined.

In contrast to modern microstructural, physical, and chemical studies of wood, the research focused on mapping the mesostructure and examining and analyzing the annual growth rings relies primarily on simple optical methods, where the difference in reflectivity of early and late wood is utilized to retrieve raw measurement data. These methods are used both to determine the nature of wood and estimate its strength and other service properties and to extract dendrochronology and dendroclimatology data. It should be stressed that purely geometrical and morphological characteristics of the studied objects, such as the width of annual growth rings, fractions of early and late wood, variations of these parameters from one ring to another, etc., are retrieved using these methods. Multiple attempts at improving the optical dendrochronology methods (primarily by modifying the sample preparation techniques, substituting while light with blue one, and applying machine vision and mathematical data processing techniques) have been made (see, e.g., [4,42–45]). However, in spite of all this, the capabilities of an approach based on photographic imaging and analysis of the image of a transverse section remain rather limited, since the reflective optical properties of wood are fairly variable and are related ambiguously or (very weakly) to other physical characteristics (specifically, mechanical characteristics) of this material.

Several attempts at applying modern physical methods (specifically, synchrotron scattering [7], 3D X-ray computer tomography [46–49], and magnetic resonance tomography [50]) to spatial mapping of the properties of wood have already been made. However, since these methods are complex, laborious, and require expensive or unique equipment, they are used only rarely. The X-ray densitometry technique is simpler, but it requires access to both sides of a planar sample cut out strictly perpendicularly to the major axes of cells and vessels [51].

In the present study, a simple method for scanning a transverse wood section with the use of modern nanoindentometry (NI) is detailed. This method provides an opportunity to measure nano/microhardness H, Young's modulus E, and other local mechanical characteristics [27–34] automatically in accordance with a preset program at several hundred predefined points on the sample surface (i.e., map mechanical properties). The proposed approach has several advantages over the traditional one based on the analysis of a transverse section image: it excludes the human factor and allows one to obtain unbiased information on local physical and mechanical properties with high resolution (up to several nanometers or several tens of nanometers if necessary), which may then be used for various purposes. Specifically, the obtained data may help, first, gain a deeper understanding of the nature and mechanisms of formation of macromechanical properties of wood and fiber (in particular, cellulose-containing) composites in relation to their microstructural characteristics; second, optimize the technologies of growth and hardening and the conditions of subsequent application of wood and composites containing natural fibers; and third, develop new independent quantitative dendrochronology and dendroclimatology methods to supplement or substitute the traditional ones.

The specific goals of the present study were to reveal the distribution of effective values of Young modulus E and hardness H within annual growth rings and layers of early

and late wood and determine their boundaries and width by NI.

1. Materials and methods

Materials to be studied were sampled in June–September 2021 in the course of selective sanitation cutting in natural forest stands in the Central Black Earth Region of the Russian Federation. Sections of common pine (*Pinus sylvestris L.*) 110–125 years of age came from the Vernadskoe forest district of the Tambov Region (Tsna forest expanse), while sections of common oak (*Quercus robur*) 90–110 years of age and small-leaved lime (*Tilia cordata*) 70–90 years of age were delivered from the scientific-experimental forestry of the Morozov Voronezh State University of Forestry and Technologies (Pravoberezhnoe forest district).

Samples for study were $30 \times 30 \times 100$ mm in size and were cut out from transverse sections of wood and dried to a moisture content of 10–12% in a drying chamber in the soft mode at a temperature of 75°C. This procedure took 24–72 h to complete. The surface preparation involved mechanical grinding and polishing performed using a Buhler (USA) polisher and abrasive materials with their grain size decreasing after each processing stage. Roughness R_a of the treated surface was measured with a di Innova (Veeco-Digital Instruments, USA) scanning probe microscope. The typical R_a value was 250–300 nm for pine and lime samples and 140–180 nm for oak. The microstructure of samples was monitored with a Tescan Vega 3 scanning electron microscope (SEM). The surface for SEM studies was prepared by removing a thin wood layer from the transverse section of polished samples with the use of a microtome. Typical images of the annual growth rings and the cell structure in the studied samples are presented in Fig. 2.

The mechanical properties of selected wood samples were mapped using a Triboindenter TI-950 (Hysitron, USA) nanoindentometer (NI). This setup is essentially a precision nano/micromechanical testing machine that records the $P-h$ (load–deformation) diagram with a rated resolution of ~ 50 nN in force P and ~ 0.5 nm in displacement h upon indentation of a sharp (the curvature radius at the apex is 20–50 nm) triangular diamond Berkovich indenter into the sample surface. The provided software allows one to program the working loading–unloading cycle (temporal force profile), and the precision computer-controlled triaxial table provides an opportunity to map the mechanical properties by scanning over multiple points (up to $\sim 10^3$) with preset coordinates on the sample surface without further intervention of the operator. Measurements were performed in accordance with the recommendations of ISO 14577 [52] and GOST 8.748-2011 [53] for NI. In the present study, maximum load $P_{\max}$ applied to the indenter was set to 500 mN. With this load, the depth of indentations was 1.5–2 orders of magnitude higher than roughness parameter R_a. These raw data were processed using the Oliver–Pharr method [54–56], which is included into international and Russian standards [52,53], to retrieve the values of H and E.

It should be noted that the lateral size of the deformation zone (80–130 μm) corresponding to the chosen maximum load $P_{\max} = 500$ mN was 3–5 times greater than the lateral size of cells. As a result, the mechanical characteristics were averaged over 10–25 neighboring cells (cell walls and capillaries included). The values of H and E measured this way may be regarded as effective ones for a given wood layer. Each point in the plots is the result of averaging of 5–10 individual measurements carried out for independent indentations under the same conditions and at the same distance from the origin of a new annual growth ring.

As is known, early (EW) and late (LW) wood may be distinguished in the structure of each annual growth ring in wood of any type. Early wood forms in spring and is characterized by low density and strength values, while late wood formed in summer and autumn has a somewhat higher density and much better mechanical characteristics. The intentionally chosen indenter load value of 500 mN (and the corresponding lateral size of the local deformation zone) allowed us to reduce the spread of H and E values compared to the data [57,58] obtained with a much lower indenter load $P_{\max}$ (2 mN), while preserving the capacity to plot E and H distributions within individual annual growth rings reliably based on a limited number of indentations. Analyzing these distributions, one may not only determine the exact position of boundaries of annual growth rings and their width, but also distinguish between intraring wood layers. This makes it possible to relate the mechanical properties within each annual growth ring both to yearly variations of the growth conditions and to variations occurring within a growth season. Traditional methods of examination based on image analysis do not provide such an opportunity. This technique may find application in dendrochronology and dendroclimatology and supplement or substitute the traditional methods, which are based on variations of the optical properties, with objective quantitative measures that contain, in addition to the data on purely geometrical characteristics of the wood structure, information on the mechanical properties of wood.

Macroscopic mechanical properties were determined in accordance with the Brinell procedure by indenting a ceramic sphere with a diameter of 12.7 mm into the end face of the transverse section of a tree trunk to a depth of 1 mm. The deformation zone extended over several annual growth rings in this case. This allowed us to compare the macroscopic and microscopic hardness values obtained for the same sample and check them against literature data.

2. Experimental results

Typical raw data in the form of $P-h$ diagrams obtained in the process of indentation of three studied types of wood are presented in Figs. 3, *a*, 4, *a*, and 5, *a*. These diagrams

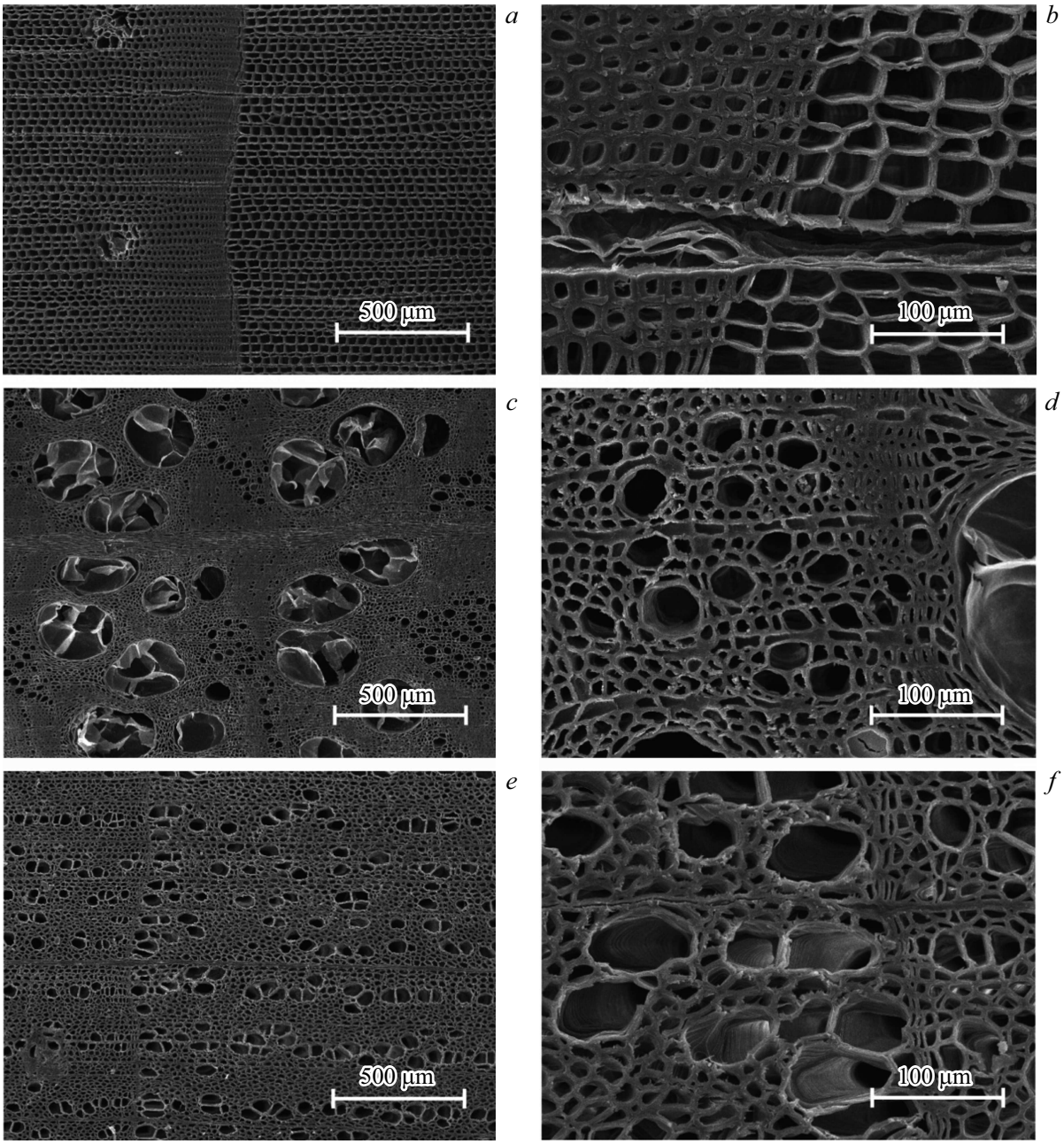

Figure 2. SEM images of the transverse section of samples of common pine (a, b), common oak (c, d), and small-leaved lime (e, f) under two magnifications. The boundaries between annual growth rings, which are characterized by a jump-like change in the morphology and the size of cells and tracheids, are aligned vertically.

are similar to $\sigma-\varepsilon$ (σ is stress and ε is relative strain) curves, which are used widely to study and characterize macroscopic mechanical properties of materials, but are recorded with a nanometer resolution. $P-h$ diagrams contain data on elastic, plastic, and viscoelastic properties of the studied material, its Young's modulus, hardness, creep rate, strain-hardening coefficient, and other physical and mechanical characteristics that may be retrieved using different methods (specifically, the most commonly used Oliver–Pharr method [54–56]). The nanometer resolution in h allows one to record and analyze elementary deformation events in the region that is localized under the indenter and grows continuously as the pyramidal indenter penetrates into the material to a depth growing from several nanometers to several hundred micrometers. The key results on the determination of the radial dependence of H and E in transverse sections of wood are presented in Figs. 3, *b*, 4, *b*, and 5, *b*. It is evident that the local mechanical properties of all three types of wood are markedly periodic. Jump-like E and H changes are consistent with the positions of boundaries of annual growth rings identified optically by detecting changes in the color of wood. The values of E

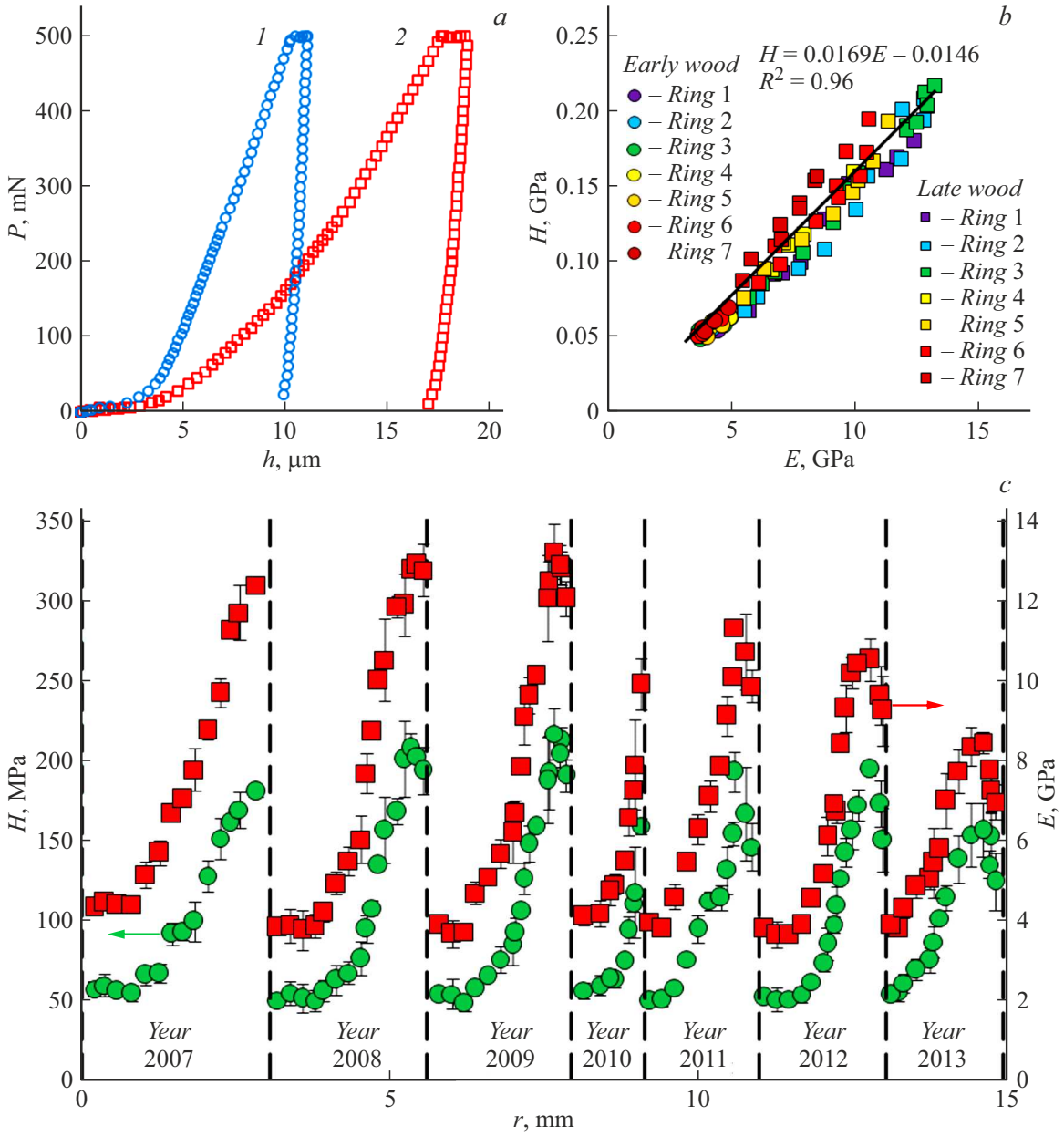

Figure 3. Micromechanical properties of annual growth rings of common pine wood studied by scanning nanoindentation with the maximum load applied to a Berkovich indenter being equal to $P_{max} = 500$ mN. *a* — typical $P-h$ diagrams for late (*1*) and early (*2*) wood; *b* — dependences of hardness H on Young's modulus E for seven consecutive annual growth rings; *c* — dependences of H and E on distance r measured transverse to annual growth rings (for seven consecutive rings). The boundaries of annual growth rings are indicated with dashed lines.

and H within annual growth rings vary smoothly in pine and lime in transition from EW to LW and change abruptly in oak. Linear relations between E and H with almost the same slope coefficient $m = 0.017 \pm 0.002$ were observed in all three types of wood (Figs. 3, *c*, 4, *c*, and 5, *c*). In other words, ductility ratio $\mathrm{DR} = E/H$ was approximately equal to 60 in all samples. This is typical of many types of wood (e.g., DR for eucalypts falls within the range from 54 to 68 [59] with a mean value of 61, and beech wood has $\mathrm{DR} \approx 55$ [60]).

The values of H and E within each EW layer vary only slightly ($\sim 10\%$) from one annual growth ring to the other and within the same ring, although the weather conditions differed substantially from one year to the other. For example, the year 2010 was very dry; this left an evident mark on annual growth ring width w (specifically, w in pine decreased by a factor of more than two compared to previous years), but had almost no effect on the values of H and E (Fig. 3, *b*) in EW. The transverse size of cells in different annual growth rings also did not vary

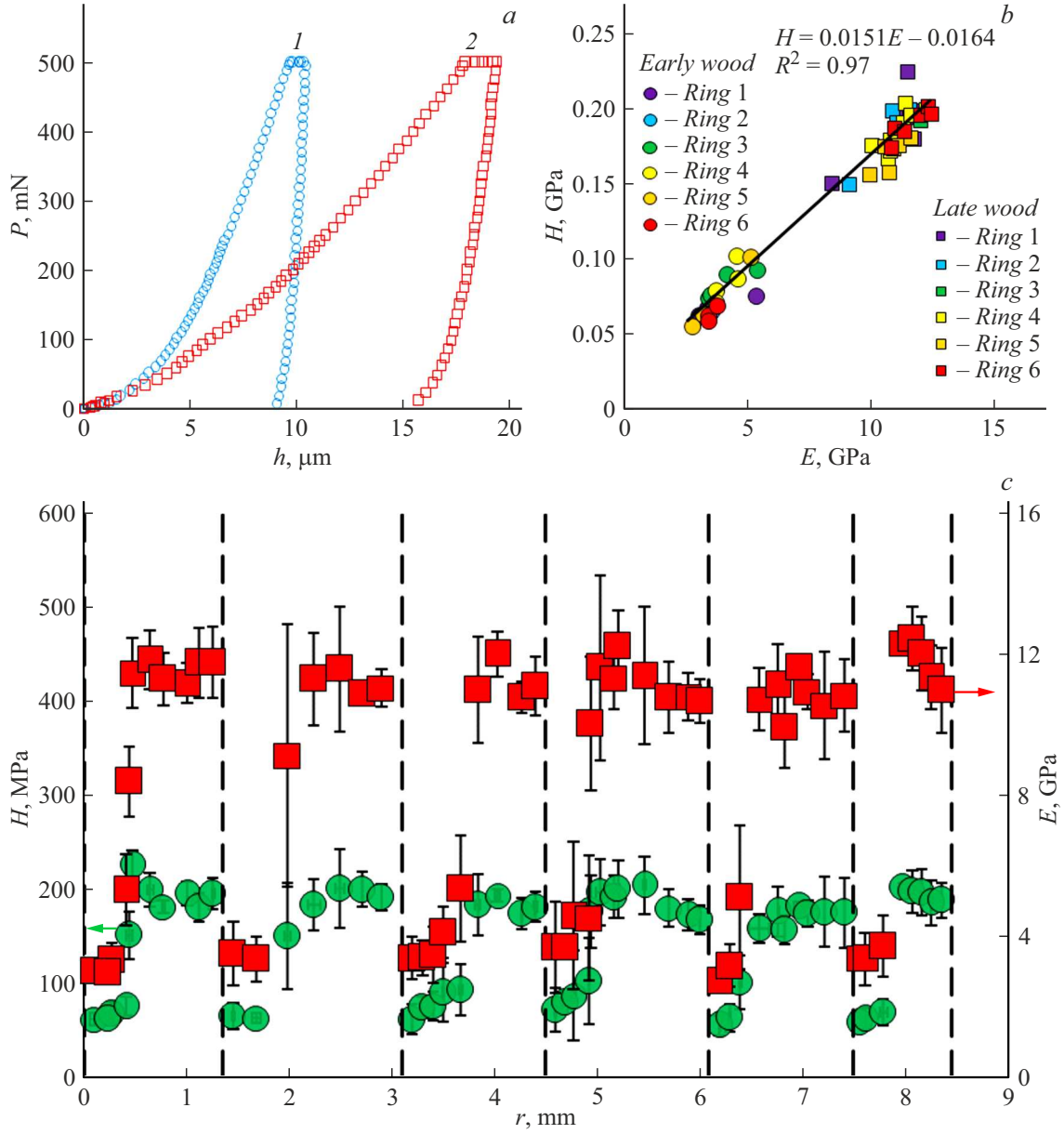

Figure 4. Micromechanical properties of annual growth rings of common oak wood studied by scanning nanoindentation with the maximum load applied to a Berkovich indenter being equal to $P_{max} = 500$ mN. *a* — typical $P-h$ diagrams for late (*1*) and early (*2*) wood; *b* — dependences of hardness H on Young's modulus E for six consecutive annual growth rings; *c* — dependences of H and E on distance r measured transverse to annual growth rings (for six consecutive rings). The boundaries of annual growth rings are indicated with dashed lines.

radically in EW, although the thickness of cell walls differed considerably (Fig. 2). Thus, the width variations of annual growth rings are mostly attributable to changes in the number of cells, which differ only slightly in size and mechanical properties, in a layer.

The differences in mechanical properties in EW and LW in several typical annual growth rings are presented in the summary table. It can be seen that the averaged value of E in LW is higher than the one in EW by a factor of 3.1 in pine, 3.5 in oak, and 1.3 in lime. The difference in hardness of LW and EW is of the same order of magnitude: 3.7-fold in pine, 3.0-fold in oak, and 1.6-fold in lime. Such ratios are, on average, typical of adjacent annual growth rings as well, although the magnitudes of differences in a specific year may deviate substantially from the average ones. For example, the hardness of EW in the 5th and the 6th rings in oak is approximately 3 times higher than H in previous rings, while the hardness of LW remains approximately the same. It is evident that such discrepancies are attributable to the specifics of climatic conditions in these anomalous periods. This is also evidenced by the fact that the fifth and the sixth annual growth rings are

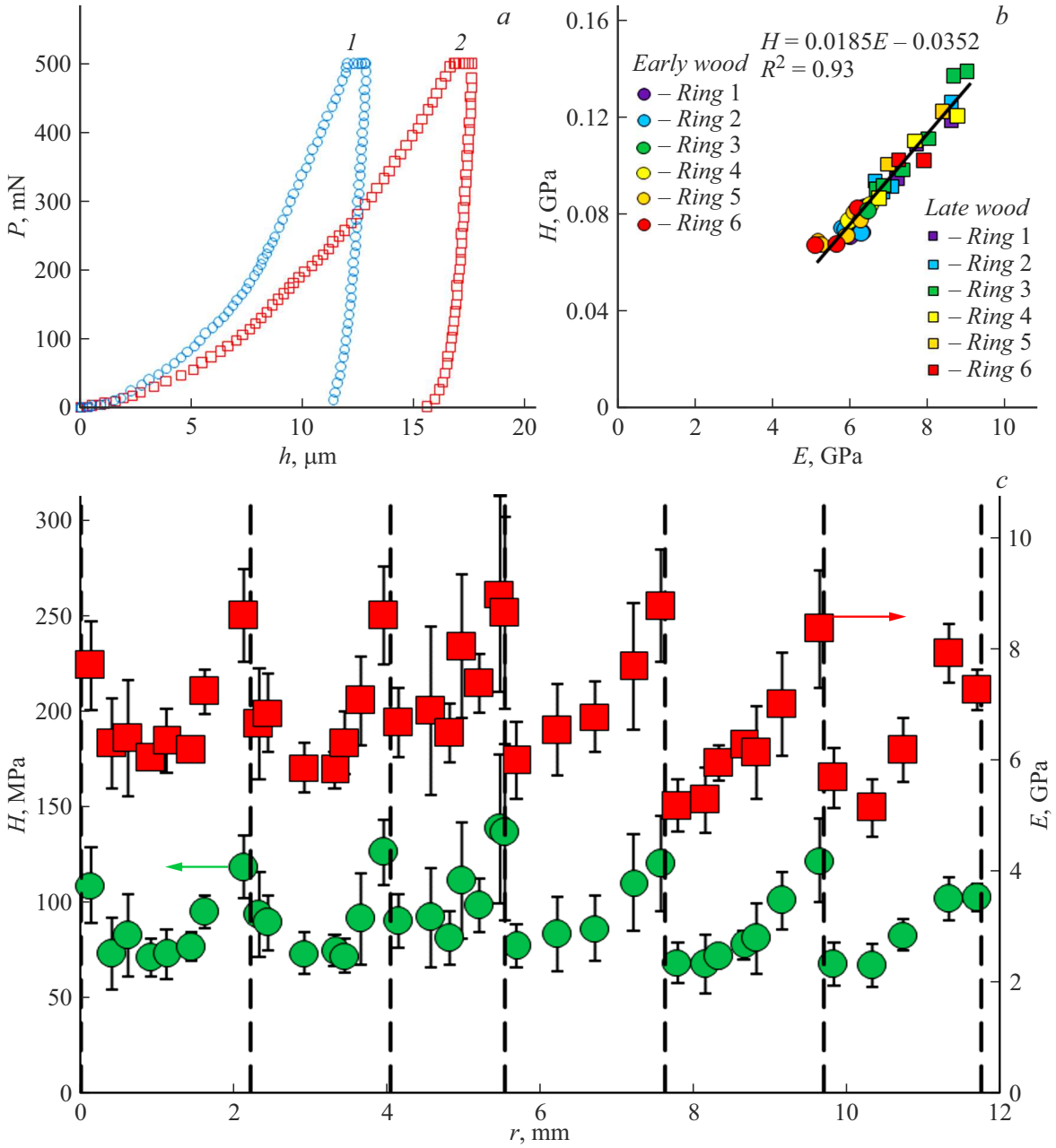

Figure 5. Micromechanical properties of annual growth rings of small-leaved lime wood studied by scanning nanoindentation with the maximum load applied to a Berkovich indenter being equal to $P_{max} = 500$ mN. *a* — typical $P-h$ diagrams for late (*1*) and early (*2*) wood; *b* — dependences of hardness H on Young's modulus E for six consecutive annual growth rings; *c* — dependences of H and E on distance r measured transverse to annual growth rings (for six consecutive rings). The boundaries of annual growth rings are indicated with dashed lines.

thinner. However, the yearly variation of hardness is much greater than the difference in ring thickness that is often used to gauge retrospectively the variations of climatic conditions. This implies that the measurement of hardness with a high spatial resolution may be a much more sensitive and accurate method of dendroclimatology than the measurement of width variations of annual growth rings.

The mechanical properties of LW are weakly sensitive to the growth conditions and the width of annual growth rings in pine (Fig. 6) and almost insensitive to these parameters in oak (Fig. 7) and lime. In the case of EW, the dependence was also lacking in all the studied annual growth rings.

Let us discuss another important mechanical parameter of wood: nanohardness H_c of cell walls. It varies only slightly among different layers and annual growth rings (and even different types of wood). Let us cite the results of several studies where nanohardness H_c of cell walls in the longitudinal direction was determined by NI. The values

Mechanical characteristics of structural elements of pine, oak, and lime wood at different scale levels

Number research died annual ring	Micromechanical properties (results obtained by nanoindentation)					Macromechanical properties				
						Measured in the study	Tabular			
	Fraction of late wood m, %	Early wood		Late wood			Average, without separating into early and late wood		Early wood	Late wood
		E_e, GPa	H_e, MPa	E_l, GPa	H_l, MPa	H_B, MPa	E_t, GPa	H_t, MPa	H_{et}, MPa	H_{lt}, MPa
Common pine (Pinus sylvestris)										
1	26.6	4.39±0.04	56.7±1.6	12.35±0.68	180.1±10.9	44.1±4.6	12.1 [66] 11.3 [68]	27–31 [67] 27 [69]	20.6 [68]	105.4 [68]
2	38.8	3.89±0.12	52.3±2.3	12.78±0.28	201.2±9.1					
3	34.8	3.75±0.25	51.9±5.7	12.78±0.69	212.2±4.3					
Common oak (Quercus robur)										
1	65.2	3.09±0.16	63.7±2.6	11.07±0.77	189.3±16.2	66.6±3.6	14.3 [66]	25–42 [67]	52.4 [68]	92.7 [68]
2	63.2	3.42±0.07	63.9±1.3	11.14±0.27	196.6±3.9					
5	65.5	2.93±0.22	58.8±3.9	10.81±0.39	172.8±5.5					
Small-leaved lime (Tília cordáta)										
1	34.9	6.68±0.14	75.4±3.5	8.59±0.84	118.4±16.4	46.5±2.5	–	19 [69]	–	–
2	32.9	5.99±0.21	73.5±0.9	8.59±0.88	126.3±16.9					
3	48.6	6.68±0.14	87.9±4.3	8.81±0.17	137.6±0.9					

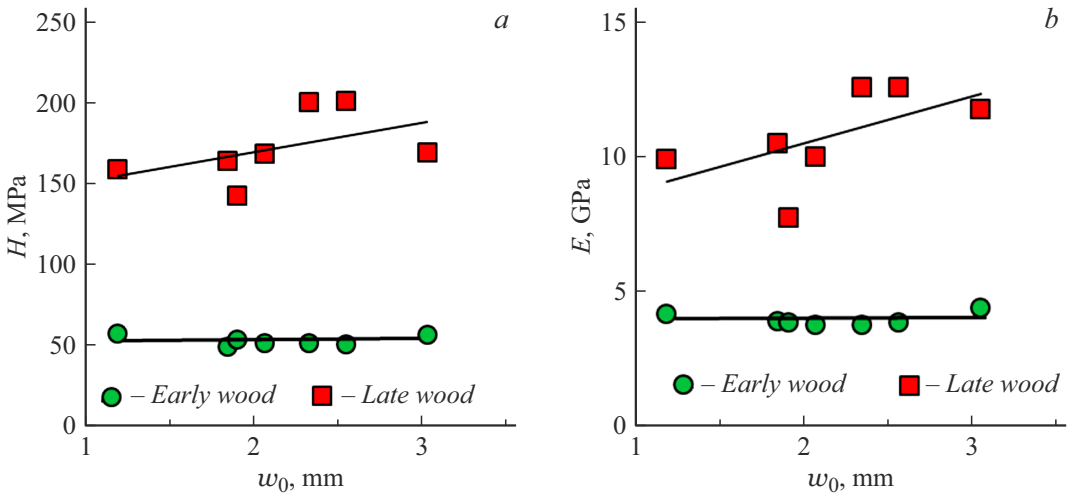

Figure 6. Dependences of hardness H (a) and Young's modulus E (b) for early and late wood of common pine on width w_0 of an annual growth ring measured optically.

of H_c determined in [40] in juvenile common pine (Pinus sylvestris L.) wood (the 7th annual growth ring) were 439 MPa in EW and 466 MPa in LW; in mature wood (the 74th annual growth ring), the nanohardness was 469 MPa in EW and 489 MPa in LW. The hardness of cell walls in pine (Pinus massoniana Lamb.) wood in [61] varied within the 0.35–0.42 GPa range regardless of whether the cell lumen was filled with plastic in the course of coating with a lacquer or not. The authors of [62] reported a cell wall hardness in Masson pine wood of 0.41–0.53 GPa and found no difference between EW and LW within the spread of data, and the authors of [63] examined loblolly pine (Pinus taeda) wood and found $H_c = 0.34–0.54$ GPa (without differentiating into early and late wood).

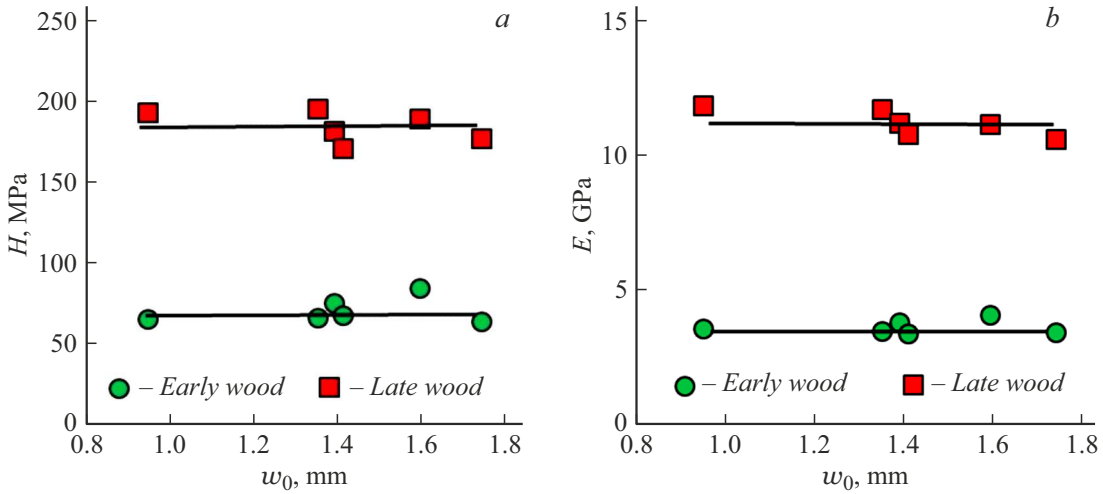

Figure 7. Dependences of hardness H (a) and Young's modulus E (b) for early and late wood of common oak on width w_0 of an annual growth ring measured optically.

The above data on H_c suggest that the structures of cell walls of different layers and types of wood are similar. The relative differences between them are significantly smaller than the corresponding differences for effective macroscopic parameters E and H measured in our experiments, Brinell macrohardness H_B, and tabular macroscopic properties. However, the absolute value of H_c is always higher than the absolute value of microhardness H measured in the present study (and certainly higher than the values of macrohardness and macrostrength). This may be regarded formally as a manifestation of the size effect (SE) in the mechanical properties of wood. However, the issue of determination of specific fractions of this SE attributable to solid wood and to pores warrants a separate study.

3. Discussion

Consistent data on the nature of physical and mechanical properties and size effects in wood at different scale-hierarchical levels are rather scarce. Let us review the most interesting typical data. The calculated strength of elementary cellulose nanocrystals and nanofibrils 3–15 nm in diameter is 4.9–10 GPa [1]. The results of processing of Raman spectra and three-point bending tests with atomic force microscopes agree with these values [2]. The strength of microfibers 8–12 μm in diameter is approximately an order of magnitude lower: 0.8–1.57 GPa [36,37,64]. The nanohardness of cell walls with a typical thickness of 2–5 μm falls within the 0.3–0.6 GPa range [38–41,59,65]; i.e., it is 3–5 times lower than the strength of cellulose microfibers. It follows from the table that the local values of H measured by NI in our experiments were several (2–4) times lower than the nanohardness of cell walls in all three types of wood both in EW and in LW layers. At the same time, the measured H value was several times higher than Brinell macrohardness H_B measured for the same samples and than the reference values of hardness and uniaxial tension strength obtained in macrotests [66–69]. These data agree with the results of [70], where Brinell macrohardness $H_B = 0.029 \pm 0.005$ GPa of jack pine (Pinus banksiana Lamb.) was found to be an order of magnitude lower than the average microhardness of cell walls ($H = 0.297 \pm 0.034$ GPa). The mechanical properties of beech wood in [60] were also measured at two scale levels: in cell walls (by NI) and in annual growth rings (by Brinell indentation of a sphere 2.5 mm in diameter with the application of force $P_{max} = 100$ N). It was found that $H_c = 400–500$ MPa was almost an order of magnitude higher than $H_B = 65–70$ MPa. It is evident that the above-described degradation of mechanical characteristics with an increase in characteristic size R^* of the studied object may be regarded as a natural corollary of SEs detected in various types of wood. They are phenomenologically similar to SEs that are observed in metals and alloys, ceramics, and composite materials and characterized by the Hall–Petch relation: $\sigma_y = \sigma_0 + A(R^*)^{-0.5}$, where σ_y is the yield stress and σ_0 and A are material constants. Similar relations are valid for hardness. Naturally, the reasons behind the hardness and strength reduction with an increase in R^* in different groups of materials, just as in nano/microcellulose, cell walls, and layers of early and late wood, may differ. Their mechanisms require separate study. At the same time, these SEs may also have common causes.

For example, it is evident that the reduction in the effective Young's modulus and hardness at meso- and macrolevels is affected strongly, in addition to the internal mechanisms governed by the molecular and supramolecular structure of nanofibrils and cellulose microfibers, by the nano- and microporosity of wood that is associated with the presence of pores, capillaries, and larger tracheids with a greater aspect ratio. These structural features account for several significant differences in mechanical behavior

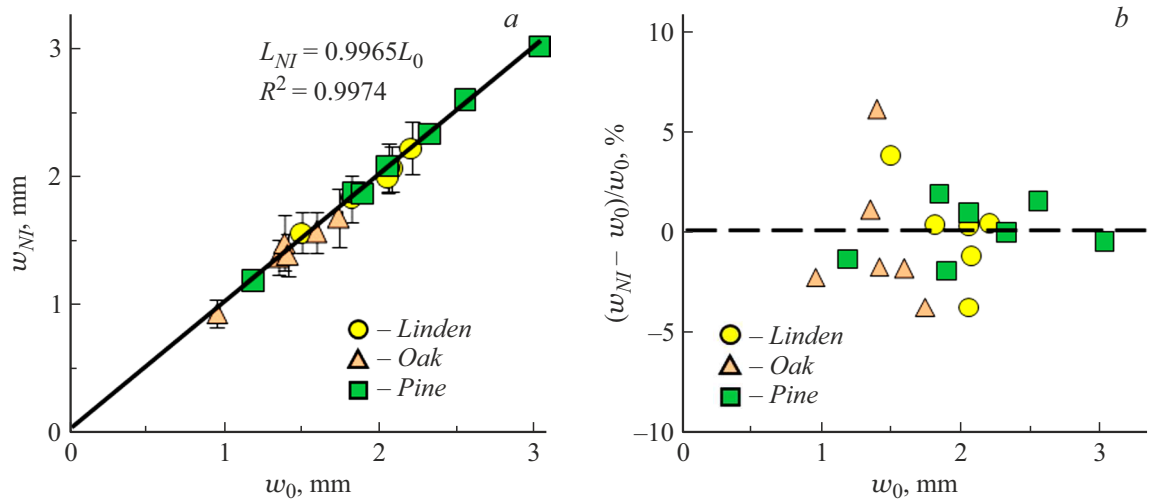

Figure 8. Results of measurement of the width of annual growth rings by nanoindentation w_{NI} and optically w_0 (a) and deviations between these methods (b).

between wood and solid materials. First, the Tabor rule, according to which the yield or ultimate strength is approximately equal to the hardness of soft materials divided by 3, is almost always violated. In contrast, the macrohardness of most types of wood is typically several times lower than the yield or ultimate tensile strength. Apparently, all such phenomena are attributable to the loss of stability of the honeycomb structure of wood under indentation and uniaxial compression that occurs much earlier than inelastic deformation and breaking under tension. In view of the anisotropy of mechanical properties of wood, these phenomena depend strongly on the direction of application of load relative to the major axis of cells and tracheids. Whatever the case might be, it follows from the table and literature data that wood features well-marked SEs, which are manifested in the reduction of strength/hardness from ~ 10 GPa in nanocrystalline cellulose to ~ 0.1 GPa in macroscopic volumes of wood. This implies that all cellulose-containing materials have strong potential for hardening, which may be unleashed by optimizing their nano- and microstructure via the application of appropriate techniques.

4. Application in dendrochronology

The presence of an abrupt hardness jump at the boundaries of annual growth rings allowed us to determine their width w_{NI} based on the scanning NI data. The obtained values were then compared to width w_0 that was determined optically (based on the photographic image contrast) using a method similar to the one applied in common LINTAB equipment. The results of comparison of these two methods for determination of the width of annual growth rings are presented in Fig. 8. It can be seen that the differences between them are no higher than 2–3% in pine wood and do not exceed 4–5% in oak and lime. The deviation averaged over 6–7 rings was approximately two times lower. This essentially implies that the scanning indentation method may serve as an alternative to the optical one or provide supplementary data on the local mechanical properties.

Conclusion

Scanning indentation with different maximum loads makes it possible to obtain multiscale data on the mechanical properties of wood at different structural levels (from nano- to the macrolevel). The comparison of detailed data on the distribution of mechanical characteristics within an annual growth ring and in adjacent rings with macroscopic characteristics provides an opportunity to gain a better understanding of the nature and mechanisms of formation of macroparameters. This, in turn, may offer new approaches to optimization of the growth conditions of wood with predetermined mechanical properties (e.g., high strength and elasticity, needed acoustical characteristics, or low creep rate) and to the development of physically grounded methods of wood hardening.

It is important to note that the proposed method of scanning without preselection of indentation points and targeting of cell walls, the chosen value of $P_{\max} = 500$ mN, and the simplified surface treatment procedure, which leaves a fraction of ground microfibers in capillaries of the sample prepared for measurements, do not preclude one from determining the effective E and H values and even have several advantages over the earlier methods for E and H measurement in individual cell walls at much lower $P_{\max}$ values. First, this technique allows for high-throughput inspection of large surface areas ($\sim 10^4$ mm^2 and greater instead of just several mm^2 prepared with a microtome) second, the ratio of effective microhardness values in LW and EW (with the influence of porosity and capillaries

and their partial filling with polishing products taken into account) is much higher than the ratio of E and H values in cell walls in LW and EW. The above implies that the measurement of effective H and E values may be a much more sensitive method of dendrochronology and dendroclimatology than the use of local H and E values in cell walls and the measurement of width variations of annual growth rings.

The method of $1D$ scanning NI in the radial direction or $2D$ mapping of a transverse trunk section may serve as a highly informative alternative or supplementary (with respect to the traditional optical examination) technique for dendrochronology and dendroclimatology. In contrast to the traditional method, it provides an opportunity both to determine purely geometrical characteristics of the annular growth structure (width of annual growth rings and layers of early and late wood) and to map several intraring parameters of wood (nano- and microhardness, Young's modulus, contact stiffness, and other mechanical characteristics) with a high resolution. This makes it possible to estimate not only the average annual climatic changes, but also intraseasonal changes that are of interest for dendrochronology and dendroclimatology. Since the average size of cells in a transverse section of wood is $30-50\,\mu$m and the average width of an annual growth ring is $1-3$ mm, $50-100$ cells lie within a single ring. Nanoindentation potentially allows one to measure the mechanical characteristics of each cell. Therefore, the ultimate temporal resolution of NI applied in dendrochronology may be estimated at approximately 1 week.

Funding

This study was performed at the Common Use Center of the Derzhavin Tambov State University and was supported by grant No. 21-14-00233 from the Russian Science Foundation (examination of the distribution of local mechanical properties) and by the Ministry of Science and Higher Education of the Russian Federation as part of the project under agreement No. 075-15-2021-709, unique project identifier RF-2296.61321X0037 (sample preparation, SEM studies).

Conflict of interest

The authors declare that they have no conflict of interest.

References

[1] *Handbook of Nanocellulose and Cellulose Nanocomposites,* eds. H. Kargarzadeh, I. Ahmad, S. Thomas, A. Dufresne (Wiley-VCH Verlag GmbH & Co. KGaA, Weinheim, Germany, 2017)
[2] R.J. Moon, A. Martini, J. Nairn, J. Simonsen, J. Youngblood. Chem. Soc. Rev., **40** (7), 3941 (2011). DOI: 10.1039/C0CS00108B
[3] M. Reza, E. Kontturi, A.-S. Jääskeläinen, T. Vuorinen. Bioresources, **10** (3), 6230 (2015). DOI: 10.15376/biores.10.3
[4] A. Balzano, K. Novak, M. Humar, K. Čufar. Les/Wood, **68** (2), 5 (2019). DOI: 10.26614/les-wood.2019.v68n02a01
[5] J. Thomas, D.A. Collings. In book: *Wood is Good. Current Trends and Future Prospects in Wood Utilization,* eds. K.K. Pandey, V. Ramakantha, S.S. Chauhan, A.N.A. Kumar (Springer Nature Singapore Pte Ltd., 2017), p. 29. DOI: 10.1007/978-981-10-3115-1_3
[6] M. Broda, C.-M. Popescu. Spectrochimica Acta. Part A: Molecular and Biomolecular Spectroscopy, **209**, 280 (2019). DOI: 10.1016/j.saa.2018.10.057
[7] E.E.N. Alves, D.R.O. Rodriguez, P.A. Rocha, L. Vergütz, L.S. Junior, D. Hesterberg, L.C.R. Pessenda, M. Tomazello-Filho, L.M. Costa. Results in Chem., **3**, 100121 (2021). DOI: 10.1016/j.rechem.2021.100121
[8] J. Tintner, B. Spangl, F. Reiter, E. Smidt, M. Grabner. Wood Sci. Technol., **54**, 313 (2020). DOI: 10.1007/s00226-020-01160-x
[9] C.M. Popescu, D. Jones, D. Krzisnik, M. Humar. J. Molecular Structure, **1200**, 127133 (2020). DOI: 10.1016/j.molstruc.2019.127133
[10] N. Gierlinger. Appl. Spectr. Rev., **53** (7), 517 (2018). DOI: 10.1080/05704928.2017.1363052
[11] T. Kanbayashi, Y. Kataoka, A. Ishikawa, M. Matsunaga, M. Kobayashi, M. Kiguchi. J. Photochem. Photobiol., B: Biology, **187**, 136 (2018). DOI: 10.1016/j.jphotobiol.2018.08.016
[12] A. Saletnik, B. Saletnik, C. Puchalski. Molecules, **26**, 1537 (2021). DOI: 10.3390/molecules26061537
[13] K. Elsayad, G. Urstoger, C. Czibula, C. Teichert, J. Gumulec, J. Balvan, M. Pohlt, U. Hirn. Cellulose, **27**, 4209 (2020). DOI: 10.1007/s10570-020-03075-z
[14] X. Kang, A. Kirui, M.C.D. Widanage, F. Mentink-Vigier, D.J. Cosgrove, T. Wang. Nature Commun., **10**, 347 (2019). DOI: 10.1038/s41467-018-08252-0
[15] T. Scharnweber, A. Hevia, A. Buras, E. van der Maaten, M. Wilmking. Sci. Total. Environ, **566–567**, 1245 (2016). DOI: 10.1016/j.scitotenv.2016.05.182
[16] E. Toumpanaki, D.U. Shah, S.J. Eichhorn. Adv. Mater., **33** (28), 2001613 (2021). DOI: 10.1002/adma.202001613
[17] L.A. Donaldson. IAWA J., **40** (4), 645 (2019). DOI: 10.1163/22941932-40190258
[18] *Nanotribology and Nanomechanics. An Introduction,* ed. B. Bhushan. 2nd ed. (Springer, Berlin–Heidelberg–NY., 2008)
[19] *Nanomechanical Analysis of High Performance Materials,* ed. A. Tiwari. (Springer Science + Business Media, Dordrech–Heidelberg–NY.–London, 2014), 348 p.
[20] *Materials Characterization: Modern Methods and Applications,* ed. N.M. Ranganathan (CRC Press, Boca Raton, Florida, 2015)
[21] Yu.I. Golovin. Phys. Solid State, **63** (1), 1 (2021). DOI: 10.21883/FTT.2021.01.50395.171
[22] R. Garcia. Chem. Soc. Rev., **49**, 5850 (2020). DOI: 10.1039/d0cs00318b
[23] B.R. Neugirg, S.R. Koebley, H.C. Schniepp, A. Fery. Nanoscale, **8**, 8414 (2016). DOI: 10.1039/c6nr00863a
[24] M. Cascione, V. De Matteis, R. Rinaldi, S. Leporatti. Microsc. Res. Technol., **80**, 109 (2017). DOI: 10.1002/jemt.22696
[25] A. Melelli, O. Arnould, J. Beaugrand, A. Bourmaud. Molecules, **25**, 632 (2020). DOI: 10.3390/molecules25030632

[26] Yu.I. Golovin, V.I. Ivolgin, V.V. Korenkov, N.V. Korenkova, R.I. Ryabko. Kondens. Sredy Mezhfaznye Granitsy, **3** (2), 122 (2001) (in Russian).
[27] Yu.I. Golovin. Phys. Solid State, 50 (12), 2205 (2008). DOI: 10.1134/S1063783408120019
[28] Yu.I. Golovin. Zavod. Lab., **75** (1), 45 (2009) (in Russian).
[29] Yu.I. Golovin, *Nanoindentirovanie i ego vozmozhnosti* (Mashinostroenie, M., 2009) (in Russian).
[30] A.C. Fischer-Cripps. *Nanoindentation* (Springer, NY., 2011)
[31] *Handbook of Nanoindentation with Biological Applications,* ed. M.L. Oyen (Pan Stanford Publishing Pte. Ltd., 2011)
[32] *Nanoindentation in Materials Science,* ed. J. Nemecek (InTech, London, 2012)
[33] *Nanomechanical Analysis of High Performance Materials,* ed. A. Tiwari (Springer Science + Business Media. Dordrech−Heidelberg−NY.−London, 2014)
[34] *Applied Nanoindentation in Advanced Materials,* eds. A. Tiwari, S. Natarajan (John Wiley & Sons, NY., 2017)
[35] L.J. Gibson. J. Royal Soc., Interface, **9**, 2749 (2012). DOI: 10.1098/rsif.2012.0341
[36] M. Ioelovich. In book: *Handbook of Nanocellulose and Cellulose Nanocomposites,* eds. H. Kargarzadeh, I. Ahmad, S. Thomas, A. Dufresne (Wiley-VCH Verlag GmbH & Co. Weinheim, Germany, 2017). p. 51. DOI: 10.1002/9783527689972.ch2
[37] N. Mittal, F. Ansari, K. Gowda, C. Brouzet, P. Chen, P.T. Larsson, S.V. Roth, F. Lundell, L. Wagberg, N.A. Kotov, L.D. Soderberg. ACS Nano. **12** (7), 6378 (2018). DOI: 10.1021/acsnano.8b01084
[38] S. Rongpipi, D. Ye, E.D. Gomez, E.W. Gomez. Frontieres in Plant Sci., **9**, 1894 (2019). DOI: 10.3389/fpls.2018.01894
[39] N.V. Perepelkin, F.M. Borodich, A.E. Kovalev, S.N. Gorb. Nanomaterials, **10**, 15 (2020). DOI: 10.3390/nano10010015
[40] P. Mania, M. Nowicki. Bull. Polish Academy Sci. Tech. Sci., **68** (5), 1237 (2020). DOI: 10.24425bpasts.2020.134645
[41] A.C. Normand, A.M. Charrier, O. Arnould, A.L. Lereu. Scientific Reports, **11**, 5739 (2021). DOI: 10.1038/s41598-021-84994-0
[42] D.M. Meko, J.M. Friedman, R. Touchan, J.R. Edmondson, E.R. Griffin, J.A. Scott. Holocene., **25**, 1093 (2015). DOI: 10.1177/0959683615580181
[43] H. Gärtner, P. Cherubini, P. Fonti, G. von Arx, L. Schneider, D. Nievergelt, A. Verstege, A. Bast, F.H. Schweingruber, U. Büntgen. J. Visualized Experiments, **97**, e52337 (2015). DOI: 10.3791/52337
[44] X. Zhang, J. Li, X. Liu, Z. Chen. J. For. Res., **31** (2), 1002 (2019). DOI: 10.1007/s11676-019-01002-y
[45] R.J. Kaczka, R. Wilson. Dendrochronologia, **68**, 125859 (2021). DOI: 10.1016/j.dendro.2021.125859
[46] A. Vannoppen, S. Maes, V. Kint, T. De Mil, Q. Ponette, J. Van Acker, J.V. den Bulcke, K. Verheyen, B. Muys. Dendrochronologia, **44**, 66 (2017). DOI: 10.1016/j.dendro.2017.03.003
[47] J.V. den Bulcke, M.A. Boone, J. Dhaene, D. Van Loo, L. Van Hoorebeke, M.N. Boone, F. Wyffels, H. Beeckman, J. Van Acker, T. De Mil. Annals of Botany, **124**, 837 (2019). DOI: 10.1093/aob/mcz126
[48] M. Domínguez-Delmás. Dendrochronologia, **62**, 125731 (2020). DOI: 10.1016/j.dendro.2020.125731
[49] J. Martinez-Garcia, I. Stelzner, J. Stelzner, D. Gwerder, P. Schuetz. Dendrochronologia, **69**, 125877 (2021). DOI: 10.1016/j.dendro.2021.125877
[50] M. Moria, S. Kuhara, K. Kobayashia, S. Suzuki, M. Yamada, A. Senoo. Dendrochronologia, **57**, 125630 (2019). DOI: 10.1016/j.dendro.2019.125630
[51] K. Mayer, M. Grabner, S. Rosner, M. Felhofer, N. Gierlinger. Dendrochronologia, **64**, 125781 (2020). DOI: 10.1016/j.dendro.2020.125781
[52] ISO group TC 164/SC 3/WG1 and ASTM E28.06.11. ISO/DIS 14577-1, 2, 3.
[53] GOST R 8.748-2011. State System for Ensuring the Uniformity of Measurements. Metallic Materials. Instrumented Indentation Test for Hardness and Materials Parameters. Part 1. Test Method (in Russian).
[54] W.C. Oliver, G.M. Pharr. J. Mater. Res., **7** (6), 1564 (1992). DOI: 10.1557/JMR.1992.1564
[55] W.C. Oliver, G.M. Pharr. J. Mater. Res, **19** (1), 3 (2004). DOI: 10.1557/jmr.2004.19.1.3
[56] W.C. Oliver, G.M. Pharr. MRS Bull., **35** (11), 897 (2010). DOI: 10.1557/mrs2010.717
[57] Yu.I. Golovin, A.I. Tyurin, D.Yu. Golovin, A.A. Samodurov, I.A. Vasyukova. Russ. Phys. J., **63** (11), 2041 (2021). DOI: 10.17223/00213411/63/11/187
[58] Yu.I. Golovin, A.I. Tyurin, A.A. Gusev, S.M. Matveev, D.Yu. Golovin. Pis'ma Zh. Tekh. Fiz., **48** (4), 36 (2022) (in Russian). DOI: 10.21883/PJTF.2022.04.52083.19040
[59] I. Carrillo-Varela, P. Valenzuela, W. Gasitua, R.T. Mendoca. BioResources, **14** (3), 6433 (2019). DOI: 10.15376/biores.14.3.6433-6446
[60] S. Stanzl-Tschegg, W. Beikircher, D. Loidl. Holzforschung, **63**, 443 (2009). DOI: 10.1515/HF.2009.085
[61] Y. Wu, X. Wu, F. Yang, H. Zhang, X. Feng, J. Zhang. Forests, **11**, 1247 (2020). DOI: 10.3390/f11121247
[62] Y.H. Huang, B.H. Fei, Y. Yu, S. Q. Wang, Z.Q. Shi, R.J. Zhao. Bioresources, **7** (3), 3028 (2012). DOI: 10.15376/biores.7.3.3028-3037
[63] W.T.Y. Tze, S. Wang, T.G. Rials, G.M. Pharr, S.S. Kelley. Composites: Part A. **38**, 945 (2007). DOI: 10.1016/J.COMPOSITESA.2006.06.018
[64] J. Wang, L. Wang, D.J. Gardner, S.M. Shaler, Z. Cai. Cellulose, **28**, 4511 (2021). DOI: 10.1007/s10570-021-03771-4
[65] X. Wang, Y. Li, Y. Deng, W. Yu, X. Xie, S. Wang. BioResources, **11** (3), 6026 (2016). DOI: 10.15376/biores.11.3.6026-6039
[66] Electronic source. Available at: lesoteka.com
[67] Electronic source. Available at: extxe.com
[68] A.M. Borovikov, B.N. Ugolev. *Spravochnik po drevesine: Spravochnik,* Ed. B.N. Ugolev (Lesnaya Promyshlennost', M., 1989) (in Russian).
[69] Electronic source. Available at: les.novosibdom.ru
[70] M. Vincent, Q. Tong, N. Terziev, G. Daniel, C. Bustos, W.G. Escobar, I. Duchesne. Wood Sci. Technol., **48** (1), 7 (2013). DOI: 10.1007/s00226-013-0580-5